Observation of a shape-dependent density maximum in random packings and glasses of colloidal silica ellipsoids

2007 J. Phys.: Condens. Matter 19 376108

(http://iopscience.iop.org/0953-8984/19/37/376108)

IOP PUBLISHING JOURNAL OF PHYSICS: CONDENSED MATTER

J. Phys.: Condens. Matter **19** (2007) 376108 (16pp) doi:10.1088/0953-8984/19/37/376108

Observation of a shape-dependent density maximum in random packings and glasses of colloidal silica ellipsoids

S Sacanna, L Rossi, A Wouterse and A P Philipse

Van 't Hoff Laboratory for Physical and Colloid Chemistry, Debye Institute, Utrecht University, Padualaan 8, 3584 CH Utrecht, The Netherlands

E-mail: S.Sacanna@chem.uu.nl

Received 19 April 2007, in final form 18 July 2007
Published 8 August 2007
Online at stacks.iop.org/JPhysCM/19/376108

Abstract

We have measured the random packing density of monodisperse colloidal silica ellipsoids with a well-defined shape, gradually deviating from a sphere shape up to prolates with aspect ratios of about 5, to find for a colloidal system the first experimental observation for the density maximum (at an aspect ratio near 1.6) previously found only in computer simulations of granular packings. Confocal microscopy of ellipsoid packings, prepared by rapidly quenching ellipsoid fluids via ultra-centrifugation, demonstrates the absence of orientational order and yields pair correlation functions very much like those for random sphere packings. The density maximum, about 12% above the Bernal random sphere packing density, also manifests itself as a maximum in the hydrodynamic friction that resists the swelling osmotic pressure of the ellipsoid packings. The existence of the density maximum is also predicted to strongly effect the dynamics of colloidal non-sphere glasses: slightly perturbing the sphere shape in a sphere glass will cause it to melt.

(Some figures in this article are in colour only in the electronic version)

1. Introduction

The Bernal random sphere packing [3] is the classical model for amorphous matter and glasses composed of spherical particles or colloids. Many colloids in nature and technology, however, are non-spherical, and also in fundamental studies on model colloids, anisotropic particle shapes are becoming more prominent [4–6]. Thus it is of interest to inquire whether disordered, amorphous structures of non-spherical particles have a reference model, analogous to the Bernal sphere packing. With respect to this analogy two important points may be noted.

First, it was realized some time ago [7] that the Bernal random sphere packing is not unique: it is actually a member of a whole family of dense random packings with a density

that appears to be determined only by the particle shape [7]. Members of that family include spherocylinders [1], spheroids [2], cylinders with planar ends [8] and rigid fibers [7]; they all randomly pack (in a computer [1, 2] or under gravity [7, 8]) to a density which is set by the particle aspect ratio.

The second point in relation to spheres and non-spheres is that earlier work [7] showed the apparent trend that non-spheres always randomly pack less densely than spheres. The monotonic decrease in packing density with increasing aspect ratio could be explained by the increase of the (orientationally averaged) excluded volume that progressively 'dilutes' a random packing [7]. However, later it turned out that the Bernal packing does not represent a density maximum but that this maximum actually occurs for nearly spherical particles: Bernal packing represents a local minimum. This observation, initially found in computer simulations on spherocylinders [1], was confirmed by Donev *et al* [2] for ellipsoids. The latter authors also found in their simulations that the Bernal density is actually a singularity, with a steep density increase upon any minor change in shape from a sphere to a prolate or oblate ellipsoid.

Pioneering experimental work on random packing of colloidal ellipsoids [9], nevertheless, only showed a decrease of packing density with increasing aspect ratios. However, control of particle shape was insufficient to draw quantitative conclusions about the relation between ellipsoid shape and packing density and, moreover, at that time [9] no relevant computer simulations were available for comparison with experimental data. The primary aim of this work is therefore to investigate whether the intriguing density maximum for near-spheres in simulations can indeed also be observed for random packings or glasses of real non-spherical colloids. Essential for such an experimental study are well-defined colloidal spheroids with a controllable shape, ideally varying from a thin prolate to a sphere. Recently we developed a preparation procedure for monodisperse silica ellipsoids [10] that seemed to us suitable for this investigation of colloidal near-sphere packings.

In section 2 we describe the preparation of the silica ellipsoids, comprising a multi-step silica growth procedure to adjust the particle aspect ratio. Ellipsoid packings, obtained via a rapid density quench in a centrifuge, were also investigated on a single-particle level by confocal microscopy to check them for any positional or orientational order. Packing densities and microstructures were also compared to computer simulations (section 2.5). In section 3 we not only discuss the experimental and simulated density versus aspect ratio curve itself, but also the effect of this curve on the slow expansion rate of sediments against gravity. We end with a conjecture on the possibly drastic effect of particle shape on the dynamics of colloidal near-sphere glasses.

2. Materials and methods

2.1. Synthesis and controlled growth of ellipsoids

Starting from identical hematite seeds, silica ellipsoids with different aspect ratios (from 4.46 to 1.6) were obtained by a controlled seeded growth procedure which was repeated up to 20 times, in each step following the method described in [10]. The only modifications to the original procedure are a continuous feed of the reaction mixture with tetraethoxysilane (TEOS) using a peristaltic pump instead of discrete additions, and the use of slightly higher concentration of tetramethylammonium hydroxide (here 2 mM TMAH) for growing hollow ellipsoids [10]. These modifications ensure better particle size reproducibility and higher TEOS conversion. For confocal laser microscopy (CLSM), specially designed particles were prepared as follows. First, a 20 nm thick fluorescent silica shell was grown on the hematite seeds [10]. This shell, containing chemically bounded fluorescein-isothiocyanate dyes (FITC, $\lambda_{em} = 525$ nm;

$\lambda_{ex} = 495$ nm), is needed to obtain a template of the hematite core which is subsequently dissolved in concentrated HCl, yielding hollow ellipsoids with optimal optical properties for confocal microscopy (no more light absorption from the cores). Next, the (fluorescent) silica shell growth was continued until the particles were sufficiently large to be resolved by CLSM (which requires a shell thickness of about 75 nm), and finally an additional 55 nm layer of non-fluorescent silica was deposited on the particles. This core–shell morphology ensures that when a close-packed sediment is imaged, the intensity profiles of the fluorescent cores are always separated by a distance comparable to the resolution of the microscope along the xy plane. Therefore, even if the particles are touching, their position can be determined (figures 4 and 10(B)).

2.2. Particle characterization

2.2.1. Electron microscopy. The size and polydispersity of the particles were determined by transmission electron microscopy (TEM, Philips TECNAI-12). TEM pictures were analyzed using image-analysis software [11], counting typically 200 particles per sample. A Philips XL30 FEG scanning electron microscope was used to study the particle morphology and to image the microstructures of the same sediments as used in the packing experiments. TEM samples were prepared by dipping formfar-coated grids into dilute dispersions and allowing the solvent to evaporate, whereas for SEM analysis dried sediments were glued on a sample holder and coated with a 10 nm thick layer of platinum/palladium.

2.2.2. Electrophoresis. The zeta-potentials ζ were estimated from electrophoretic mobility measurements (Coulter DELSA 440 SX) on diluted samples at a pH of 6, a temperature of 25 °C, and an ionic strength of 500 μM $LiNO_3$ (Debye screening length $\kappa_s^{-1} = 7.5$ nm). Measurements were performed at constant electric field strength of 20 V/cm in both stationary layers of a silver cell. The electrophoretic mobilities μ_e were converted to zeta potentials using Smoluchowski's equation [12]:

$$\zeta = \frac{3\eta_0\mu_e}{2\epsilon_0\epsilon f_1(\kappa a)}, \tag{1}$$

where ϵ_0 and ϵ are the vacuum permittivity and the dielectric constant (24.3 for ethanol) respectively, η_0 is the solvent viscosity (0.11 cp for ethanol), and the function $f_1(\kappa a)$ is the Henry correction factor, which for large experimental κa ($\kappa a > 20$) can be approximated by [12]

$$f_1(\kappa a) = \frac{3}{2} - \frac{9}{2\kappa a} + \frac{75}{2(\kappa a)^2} - \frac{330}{(\kappa a)^3}. \tag{2}$$

2.2.3. Light scattering and contrast variation. Static light scattering (SLS) was performed at 25 °C using an automated set-up that scans the angle-dependent scattering intensity produced by a dilute dust-free dispersion illuminated by light ($\lambda = 546$ nm) from a mercury lamp (Oriel, model 66003). The solvents' refractive indices were measured with a Carl Zeiss Jena refractometer at 20 °C at a wavelength $\lambda = 589$ nm.

2.2.4. Mass densities. For each system the particle mass density ρ_p was determined by measuring the dispersion density ρ_{disp} as function of the particle concentration c:

$$\frac{\partial\rho_{disp}}{\partial c} = \left(1 - \frac{\rho_{solv}}{\rho_p}\right), \tag{3}$$

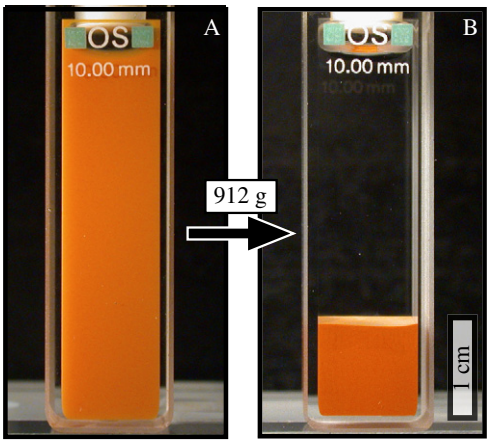

Figure 1. Initially stable dispersions of ellipsoidal particles (A) are rapidly quenched at 912 × g in a table centrifuge to obtain random close packed sediments with volumes of typically 1 cm^3 (B).

where c is in units of mass per volume (of the dispersion) and $\rho_{solv} = 0.789\,53 \pm 5 \times 10^{-5}$ g cm^{-3} is the mass density of ethanol determined, as the other densities, using an Anton-Paar (DMA-5000) density meter thermostatted at $T = 25.000\,^{\circ}C$.

2.3. Measurement of sediment densities

Densely packed sediments of ellipsoidal particles were prepared by pouring about 3 ml of stable dispersions with known weight concentration (typically 20 wt%) into optical cuvettes (Hellma, types 110-OS and 110-QS with light paths of 2 or 10 mm) and centrifuging them at 912 × g (Beckman Coulter Spinchron™ DLX) over at least 12 h. From the cuvette depth (optical path), the volume of the sediments was accurately determined from highly magnified digital pictures of the cuvette front side (figure 1) taken immediately after centrifugation with a Nikon Coolpix 5000 digital camera. To measure the sediment expansion as a function of time, samples were stored on a heavy marble table in a thermostatted (20 °C) dark room.

2.4. Confocal microscopy

Close-packed sediments of fluorescent hollow ellipsoids for confocal microscopy studies were prepared by first redispersing the particles in dimethyl sulfoxide (DMSO) (for an optimal refractive index matching) and then quenching the dispersion at high centrifugal speed ($912 \times g$) into home-made sample cells with volumes of typically 1 ml. The particles were imaged using a Nikon TE 2000U inverted microscope equipped with a Nikon C1 confocal scanning head in combination with an oil-immersion lens (100× CFI Plan Apochromat, NA 1.4, Nikon), and a ArKr laser source ($\lambda_{em} = 488$ nm). Data analysis, such as radial distribution function $g(r)$ or nearest-neighbor angle distribution function, were performed on tracked particles coordinates using image-analysis software similar to that described in [13, 14].

2.5. Simulations of ellipsoid packings

The spheroid packings were generated with the mechanical contraction method originally developed for spherocylinders [1] and later extended to simulate random packings of various other geometrical shapes [15]. Briefly the method works as follows. A gas of randomly

oriented particles is prepared in a periodic box with volume V, which is decreased in each iteration by a fixed value, and the positions of the particles are scaled so they remain inside the box. At a certain number of iterations the particles start to overlap with each other. Whether the spheroids are overlapping or not, and if so the amount of overlap, are checked using the procedure described in [16]. Any overlap between particles is removed by translating and rotating the particles using a fixed number of iterations. When it is no longer possible to remove overlaps within a reasonable amount of computer time the previous configuration of particles is accepted as the densest random packing. To find the optimal displacement an overlap removal rate is calculated and this rate is maximized by using Lagrange multipliers as described in [1, 15]. An inertia-like parameter ϵ is used to determine the ratio between translational and rotational displacement. The algorithm generates reproducible packing densities, which for spherocylinders are generally in good agreement with experimental values [1, 7].

The packing densities depend on the number of fixed iterations and ϵ. A higher number of iterations results in a denser packing. However, the number of iterations necessary to increase the density further increases exponentially until it is no longer computationally feasible to continue. Also varying ϵ leads to slightly denser packings.

3. Results and discussion

3.1. Preparation

One of the challenging aspects of this study was the preparation of a colloidal model system of non-spherical particles that would allow measuring their random packing densities as a function of only their shape. Requirements for the particles are in the first place a comparable (and low) polydispersity, a similar surface roughness, composition, charge, and mass density, to minimize their effect on the packing densities and packing microstructure. Secondly, fairly large amounts of the model colloids are needed to form macroscopic sediments (about 1 cm^3 for each sample). To meet those requirements, we prepared all our colloidal systems starting from identical seed dispersions of hematite spindles and subsequently slowly decreased the particle aspect ratio by growing, layer-by-layer, silica shells in steps of approximately 10 nm (see figure 2). The hematite cores were prepared following the procedure described in [17], which we have scaled up to a 10 litre reaction batch to obtain a sufficient amount of spindles (8.3 g of purified particles). As already shown in [10], a characteristic feature of silica growth on ellipsoidal cores is that the decrease in aspect ratio rapidly flattens with increasing silica shell thickness (figure 3), limiting the window of achievable particle aspect ratios. Figure 3 shows that, starting with hematite cores having an aspect ratio of 6.3, it is virtually impossible to achieve an aspect ratio lower than about 1.5. In figure 2 the evolution of the particle aspect ratio for some of the colloidal systems used in this study is illustrated by TEM images, whereas particle sizes and polydispersities for all the seven systems used in this study are reported in table 1.

As already mentioned in section 2.1, specially designed fluorescent hollow core–shell ellipsoids (figure 4) were prepared for confocal microscopy. We improved the original preparation method [10] by dissolving the hematite cores already in an early stage of the silica shell growth (typically once a thickness of 20 nm is reached) to limit the damage caused by HCl to the dye molecules and to achieve a higher fluorescence emission in the final sample. Another useful improvement for growing hollow ellipsoids is to employ a higher concentration of base (TMAH) to increase the TEOS conversion and reduce the number of steps needed to grow large particles. However, this is only profitable when no bare hematite core are present because of the strong tendency for ellipsoidal hematite particles (high Hamaker constant) to form, at high pH, typical heart-shape doublets or larger aggregates [7].

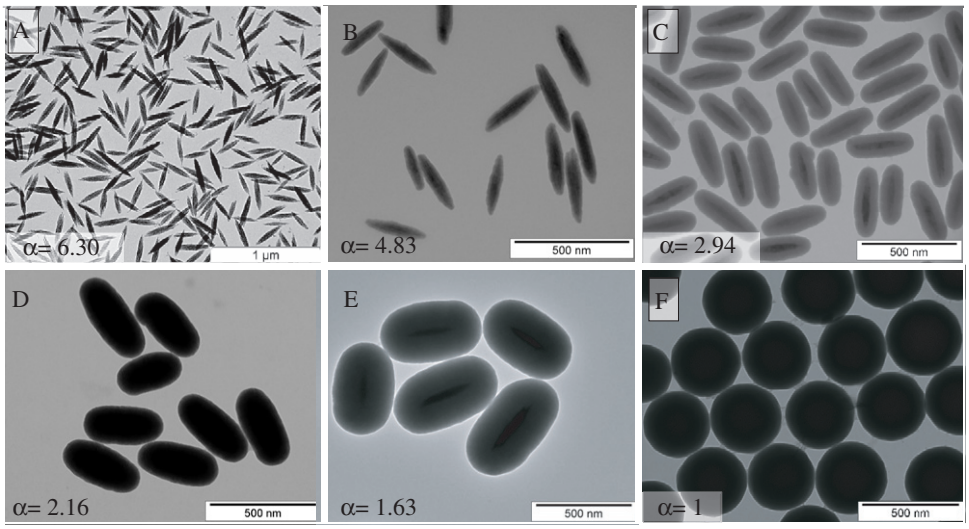

Figure 2. Starting from monodisperse ellipsoidal hematite templates having an aspect ratio of $\alpha = 6.30$ (A), we gradually changed the particle shape by a sequence of in total 20 seeded silica growth steps until $\alpha = 1.63$ ((B)–(E)). Silica spheres ($\alpha = 1$) were prepared by conventional Stöber synthesis (F).

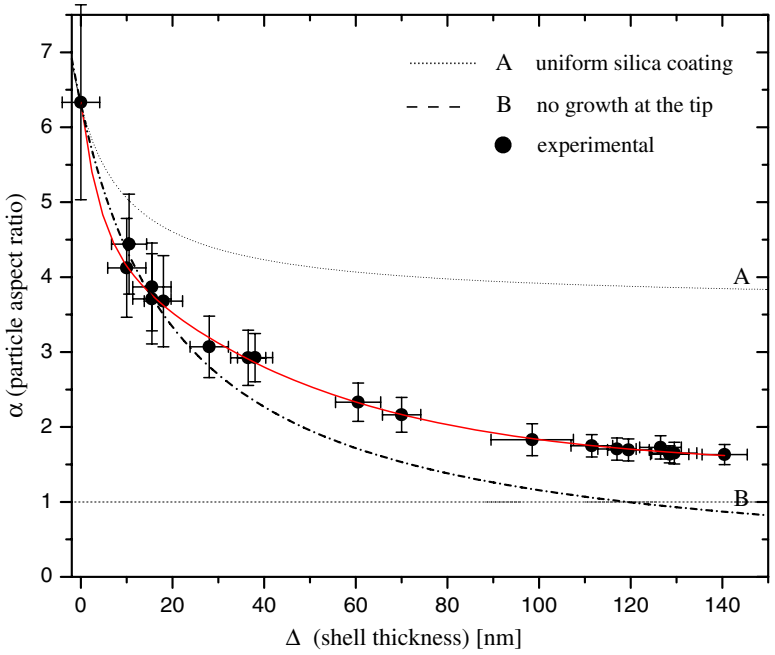

Figure 3. Decrease in particle aspect ratio due to a step-by-step silica growth on hematite seeds. The experimental results lie in between the two limiting cases [10] of an even silica deposition on the particle surface (A) and the case of no silica deposition at the particle tips (B). Fitting the data with a second-order exponential decay function (fitting line) we found a limiting aspect ratio of 1.46.

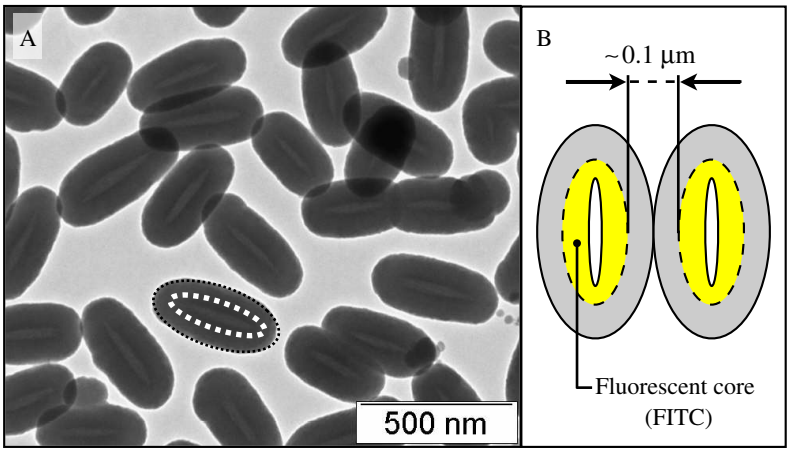

Figure 4. (A) TEM image of fluorescent core–shell hollow silica ellipsoids for confocal microscopy. The particles can be refractive index matched in DMSO due to the absence of the light-absorbing hematite core. (B) The non-fluorescent silica shell of about 55 nm allows measuring the particles' center positions even if they are touching (close-packed system).

Table 1. Properties of silica ellipsoids.

Particle aspect ratio	Particle size [a] (nm)		ρ [b] (g cm^{-3})	ϕ_{RCP} [c]	$(1-\phi)^3/\phi^2$
	Long axis	Short axis			
4.44	293 ± 38	66 ± 5	2.61	0.437 ± 0.002	0.934
3.68	298 ± 44	81± 6	2.34	0.451 ± 0.002	0.813
2.92	354 ± 35	121± 5	1.99	0.526 ± 0.004	0.385
2.16	400 ± 40	185± 6	1.98	0.585 ± 0.003	0.209
1.86	444 ± 42	239± 6	1.94	0.567 ± 0.001	0.252
1.63	532 ± 42	326 ± 8	1.85	0.607 ± 0.001	0.165
1	354 ± 28	—	2.08	0.540 ± 0.002	0.334

[a] TEM number-averaged size.
[b] Measured particle mass density.
[c] Raw experimental random close packing (RCP) volume fraction at 500 μM $LiNO_3$.

3.2. Measurement of sediment densities

For charged colloids, the packing densities strongly depend on the thickness of the electric double layer and therefore on the salt concentration in the sample. Extended double layers (low ionic strength) reduce the effective particle aspect ratio and prevent a close packing due to electrostatic repulsions. Hence, it is important to minimize those effects by using the highest ionic strength (shortest Debye length κ^{-1}) the system can tolerate before particle clustering occurs. We have studied this salt effect by monitoring the change in packing densities as a function of $LiNO_3$ concentration for ellipsoids dispersed in absolute ethanol, and also assessed how the added electrolyte affects the particle stability. For instance, ellipsoids with aspect ratio $\alpha = 1.63$ have a maximum in the packing density for 500 μM $LiNO_3$ (at higher ionic strength the particles aggregate and the sediment density decreases), whereas for spherical silica particles this limit could be raised up to 10 mM. These ionic strengths correspond to a Debye screening length κ_s^{-1} of, respectively, 7.5 and 1.7 nm in the limit of low colloid concentration.

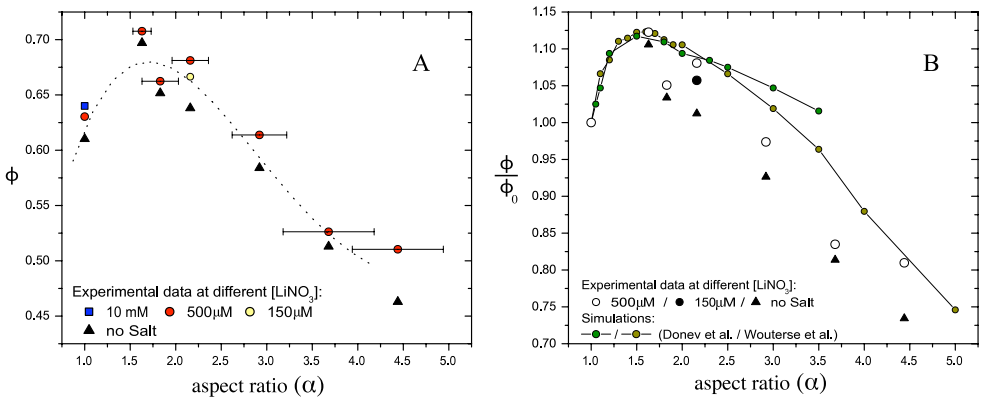

Figure 5. (A) Particle volume fractions ϕ versus aspect ratio α for randomly packed silica ellipsoids at different concentration of $LiNO_3$. (B) Reduced particle volume fractions ϕ/ϕ_0 versus α obtained from computer simulations (see [2] and [15]) compared with experimental results (ϕ_0 is the experimental random sphere packing fraction at 500 μM $LiNO_3$).

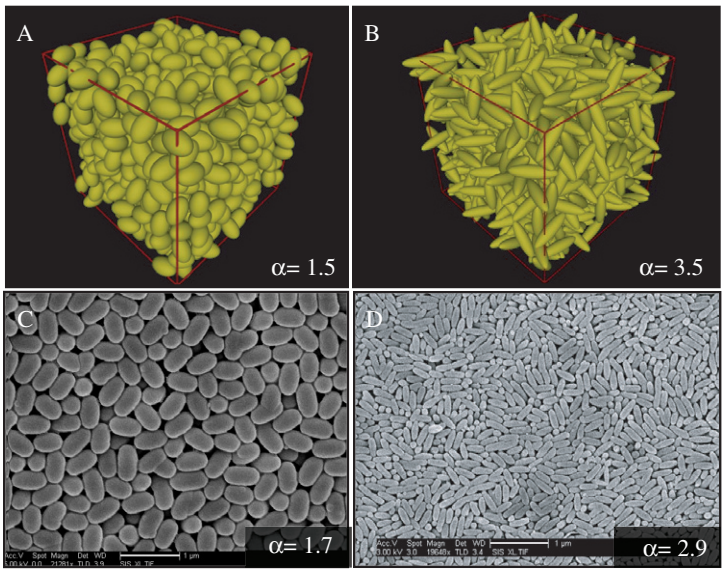

Figure 6. ((A), (B)) Computer-generated snapshot of mechanical contraction simulation of 800 spheroids with aspect ratio $\alpha = 3.5$ and $\alpha = 1.5$ compared with SEM pictures of real packings of silica ellipsoids ((C), (D)).

However, for highly concentrated suspensions the contribution of the counter-ions produced by the colloidal particles themselves (κ_c^{-1}) lowers even further the effective Debye length κ^{-1} which, assuming monovalent ions, can be estimated from [18] as:

$$\kappa^2 = (\kappa_c)^2 + (\kappa_s)^2 = 4\pi L_B n|Z^{\text{eff}}| + 8\pi L_B N_{\text{av}} c_s. \tag{4}$$

Here, L_B is the Bjerrum length, n is the colloid number density, N_{av} is Avogadro's number, and c_s is the salt concentration in units of mol m^{-3}. The effective colloid valency $|Z^{\text{eff}}|$ has been

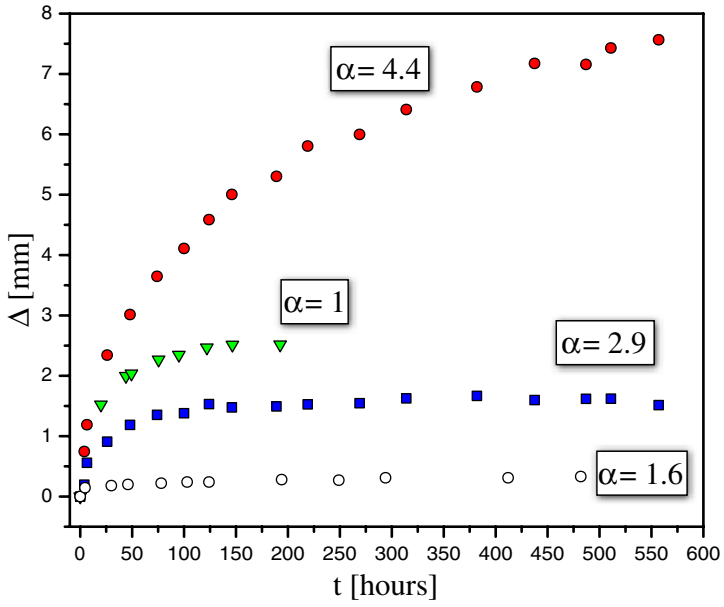

Figure 7. Expansion Δ of sediments in time (no salt added) due to the electrical double-layer repulsion between the spheroids. For the marked aspect ratio effect, see the text.

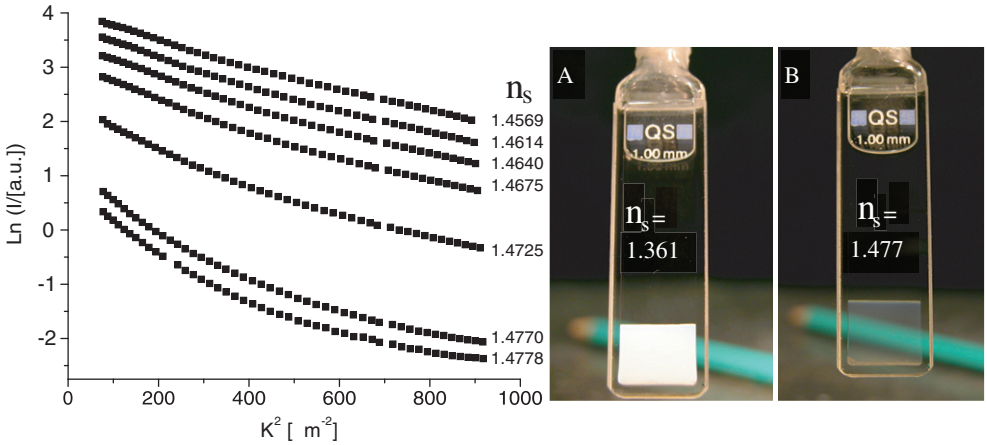

Figure 8. Guinier plots resulting from contrast variation measurements on diluted (1 wt%) dispersions of hollow ellipsoids in various DMF/DMSO mixtures ($\lambda_0 = 546.1$ nm, $T = 21.5\,^{\circ}$C). Each curve is labeled by the mixture refractive index. (A) and (B) are pictures of particle sediments in (respectively) ethanol and DMSO.

calculated from the zeta potential ($\zeta = -6.45$ mV) via the Gouy–Chapman model [19]:

$$\sigma_e = \frac{1}{e}\sqrt{8\epsilon_0\epsilon c_s RT}\,\sinh\left(\frac{e\Psi}{2k_B T}\right). \tag{5}$$

Using ζ as the surface potential Ψ, we found a particle surface charge density σ_e of 1.65×10^{-3} elementary charges per nm^2 (this is about 24 nm between two charges), and a $|Z^{\text{eff}}|$ of about 800. For packed ellipsoids in the absence of salt, this implies an electrical double layer

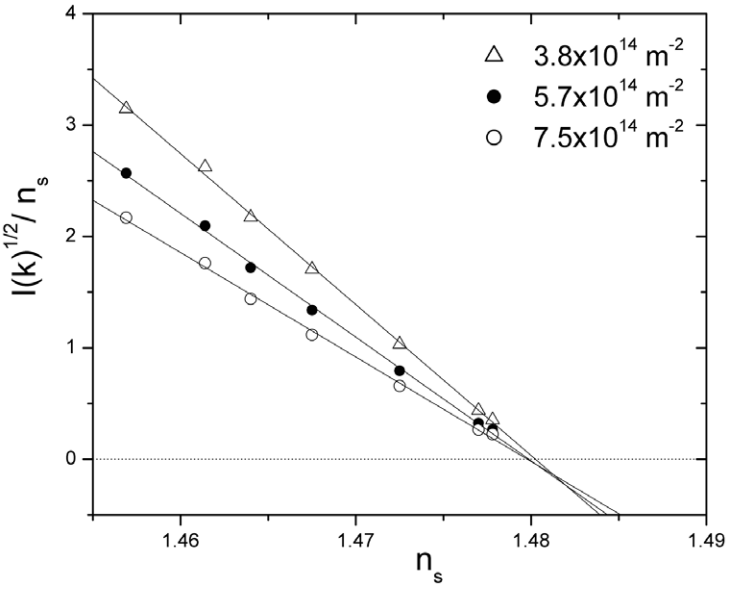

Figure 9. Extrapolation of $\sqrt{I(k)}/n_s$ to $I(k) \rightarrow 0$ for particles in DMSO/DMF for three different k-vectors as indicated in the legend. The extrapolated lines cross the x-axis at the match point n_0, which is almost independent of scattering angle, as expected for optically homogeneous particles [20].

thickness of about 46 nm, which accounts for the lower packing densities found for the samples in absolute ethanol with no salt added (figure 5). At 500 μM $LiNO_3$, κ in equation (4) is almost entirely dominated by κ_s, and the Debye screening length reduces to 7.4 nm.

The influence of the centrifugal force and centrifugation time on the packing densities and its reproducibility were also studied. However, above 1800 rpm (820 $\times$ g) we found no significant differences, and reproducible densities were obtained independently from the centrifugation time (8 or 12 h). After centrifugation all samples (with $[LiNO_3] \leqslant 500$ μM) could be redispersed to stable dispersions via prolonged immersion in a ultrasonic bath.

When particle sediments, packed in absence of added salt, are left undisturbed, the double-layer repulsions between charged particles cause a noticeable expansion of the sediments in time (see figure 7). The rate and extent of such expansion, which is largely reduced when $LiNO_3$ is present, varies with the particle shape, and it is maximal for the sample with the highest aspect ratio (figures 1 and 7), as further discussed in section 3.7.

3.3. Contrast variation

For an accurate particle tracking of the ellipsoids by confocal microscopy (see section 3.4) it is crucial to have a good matching between the refractive index of the particles (n_p) and that of the solvent (n_s) to reduce the scattering of light and therefore the blurring of the confocal image. Contrast variation measurements (figure 8) were performed by changing the optical contrast ($n_p - n_s$) of dispersions containing identical particle concentration, and recording the SLS intensity I at different wavevectors K. The contrast was varied by changing the composition of a DMSO/dimethyl formamide (DMF) mixture. Figure 8 shows that the scattering intensity in such mixtures is minimal for pure DMSO ($n_s = 1.4778$), whereas the effective particle refractive index n_p can be estimated by plotting the square root of the intensity $I(k)$ versus

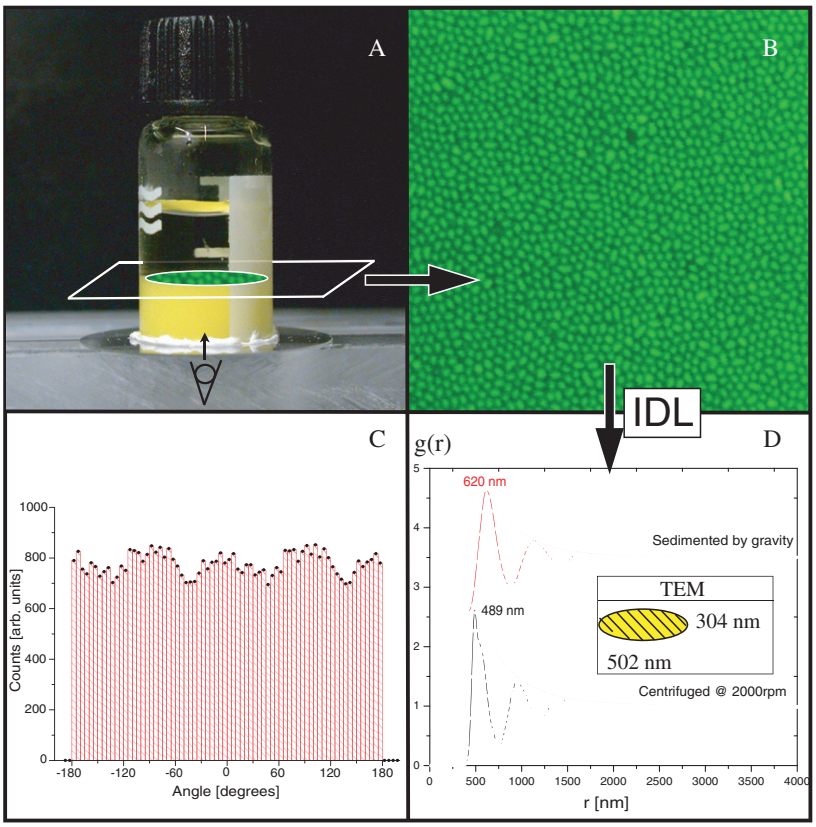

Figure 10. Optically matched packings of fluorescent core–shell ellipsoids in DMSO (A) are imaged in 2D 'slices' of 21 × 21 μm^2 by confocal microscopy (B). The corresponding 2D radial distribution function $g(r)$ (D) and the nearest-neighbor angle distribution function (C) (calculated by analyzing the center coordinates of about 20 000 particles) tell us that there is no order in the samples, confirming that the sediments in this study are indeed random packings.

n_s and extrapolating it to zero ($I(k) \rightarrow 0$) [20]. The resulting average particle refractive index ($n_p = 1.4799$) is fairly high if compared to Stöber silica (typically $n \sim 1.45$–1.46), which could be due to the adsorbed polyvinyl pyrrolidone (PVP) which was used between each growing step during the particle synthesis [10]. Moreover, the measured particle refractive index n_p is, in good approximation, independent of the scattering angle (see figure 9), which only occurs when the particles are optically homogeneous. Since we have hollow ellipsoids, this means that the solvent permeates the particles rapidly on the timescale for SLS sample preparation and measurements, and that cores always contain the same solvent composition as outside the ellipsoids.

3.4. Confocal microscopy

The effective randomness of our particle packings (i.e. absence of nematic or higher ordered phases) is confirmed by inspecting SEM images taken on dried sediments, showing no sign of a preferential orientational order (see figures 6(C) and (D)). A more quantitative study on the packing microstructure can be done by pinpointing the particle center positions in a series of two-dimensional (2D) confocal snapshots [13] taken on packings of fluorescently labeled core–shell ellipsoids. Figure 10(B) shows a representative confocal micrograph for ellipsoids

with aspect ratio 1.65 dispersed in DMSO (no salt added) and the corresponding 2D radial distribution function $g(r)$ (figure 10(D)). As expected for a random packing, we observe a short translational correlation length compared to particle size ($\xi_T = 374$ nm: envelope of $g(r) \propto \exp[\frac{-r}{\xi_T}]$), and the first peak of $g(r)$ (489 nm) being in between the long and the short particle axis dimensions (respectively $l = 502$ nm and $w = 304$ nm). When the sediments are allowed to relax in time or when the ellipsoids are settled by gravity instead of being rapidly quenched at $912 \times g$, this first peak broadens considerably and shifts to about 620 nm, indicating that the particles are still slightly repulsive despite the presence of salt. However, for our systems this relaxation time is of the order of 24 h, whereas the measurements are performed within few minutes from centrifugation. Figure 10(C) shows a nearly flat nearest-neighbor angle distribution function, which further demonstrates the absence of order in our packings.

3.5. Packing densities

Measuring absolute values of particle volume fractions ϕ is not a trivial problem since it requires knowing the correct mass densities ρ_p of the particles. Despite the fact that colloidal dispersion densities ρ_d can in principle be accurately measured (within an accuracy of 5×10^{-5} g cm^{-3}), their weight fractions are always slightly underestimated because they rely on measuring the weight fraction of dry particles (i.e. without the hydrating solvent). In figure 5(A) we have compensated for this effect by scaling the experimental packing fractions (see table 1) on the random sphere packing density of $\phi_{RCP} = 0.64$ for spherical particles packed at the highest salt concentration (Debye length $\kappa_s^{-1} = 1.7$ nm). This also facilitates the comparison with computer simulation results but, it should be noted, does not change the trend in the plot of figure 5(A), which clearly shows a maximum in the packing density for an aspect ratio around 1.6. The influence of $LiNO_3$ on the packing densities is manifest in figure 5 with a lower packing density for samples prepared in absolute ethanol with no added salt. As anticipated in section 3.2, this is the result of extensive electric double layers which prevent the particles from close packing and which tend to level off the maximum in figure 5.

3.6. Comparison to simulations

The experimental scaled volume fractions in figure 5(B) match the simulations quite well, especially near the volume fraction maximum. The volume fractions found from simulations are slightly higher, which could be due to details of the experimental packing procedure. For spheres, granular packings need to be tapped or vibrated to reach a volume fraction of 0.64 [21, 22], and it might be the case that sedimenting under high g-force is not enough to reach the densest packing in spheroids but that here also some tapping would be required to further compact the packing. A comparison of computer-generated snapshots of the simulation with SEM (figure 6) and confocal (figure 11) pictures of experimental particle packings shows in any case that the structure is very similar in both local and global structure of the packing.

A characteristic feature of simulated packings, on the other hand, that is difficult to reproduce is the steep increase in packing density very close to the sphere shape at $\alpha = 1$ (figure 5). It has been pointed out [2] that, in fact, the sphere random packing density represents a singularity. This becomes clear when both prolate (figure 5) and oblate deviation from the sphere shape are considered, showing that spheres are located at a local minimum in the form of a non-differentiable cusp [2]. There are at least two reasons why such singular behavior is difficult to observe for our colloidal spheroids. First, particles with aspect ratios in the range $1 < \alpha \leqslant 1.5$ (figure 5) need to be prepared, which is practically impossible via our silica growth procedure as explained in the discussion of figure 3. Second, even a very small

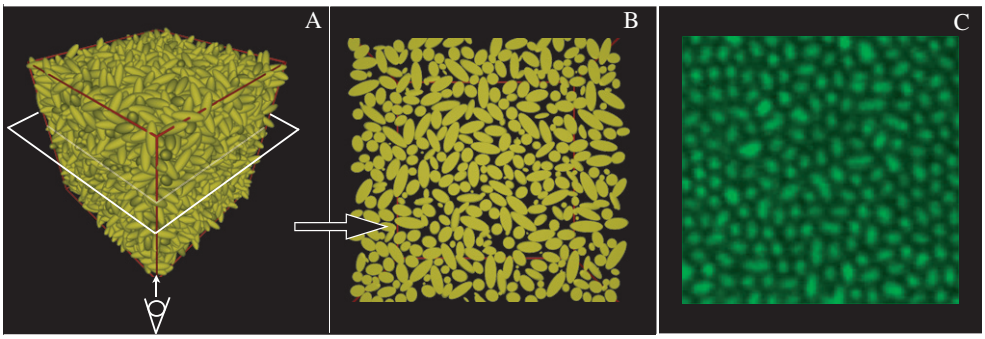

Figure 11. A 2D cross section (B) resulting from a 'virtual' cut through a simulated packing of ellipsoids (A), and a real 2D confocal image of core–shell ellipsoids (C) resemble each other closely.

polydispersity in particle size and shape (unavoidable, whatever colloid synthesis route one employs) will blur the steep gradient in packing density on approach of the sphere shape.

3.7. Sediment expansion

The rapidly quenched ellipsoid sediments (figure 1) are actually non-equilibrium systems: they slowly swell in time, as shown in figure 7. This expansion, driven by inter-ellipsoid double-layer repulsions, will continue until a sedimentation–diffusion equilibrium is reached in which the swelling osmotic pressure is balanced by gravity. Figure 7 shows that the expansion rate of the sediments strongly depends on the particle aspect ratio. This dependence can be qualitatively understood from the fact that the expansion is resisted by liquid flow along the ellipsoids and that the flow velocity will be given by Darcy's law [23] as

$$\vec{u} = -\frac{k}{\eta}\vec{\nabla} p. \tag{6}$$

Here $\vec{u}$ is the average flow velocity of an incompressible liquid with viscosity η through a porous medium (here a random particle packing), driven by an average hydrostatic pressure $\vec{\nabla} p$. The Kozeny–Carman (KC) relation for the liquid permeability is

$$k = \frac{1}{C}\frac{(1-\phi)^3}{\phi^2} A_g^{-2} \tag{7}$$

in which A_g is the specific surface area of the solid phase composing the porous medium with a solid volume fraction ϕ, and C is the so-called Kozeny constant [24]. The KC relation is known to be quite accurate for dense random packings, for spheres [25] as well as non-spherical particles, with a typical value of $C = 5 \pm 1$ for the Kozeny constant, irrespective of particle shape [23].

Taking in figure 7 the expansion of the random sphere packing ($\alpha = 1$) as reference, it is seen that the expansion rate becomes minimal for a particle shape ($\alpha = 1.6$) near the density maximum. This must be primarily due to the volume fraction term in the liquid permeability of equation (7) which is minimal at the density maximum: for the $\alpha = 1.6$ spheroids ($\phi = 0.607$) we find $(1-\phi)^3/\phi^2 \approx 0.165$, whereas for spheres ($\phi = 0.54$) the value is 0.334, corresponding to a liquid permeability which is twice as large. Beyond the maximum at $\alpha = 2.9$ the sediment volume fraction is comparable to the random sphere packing (figure 5). Nevertheless, the expansion rate for $\alpha = 2.9$ in figure 7 is still below the sphere value, presumably because the specific surface area A_g in equation (7) is higher for the $\alpha = 2.9$ spheroids which increases the

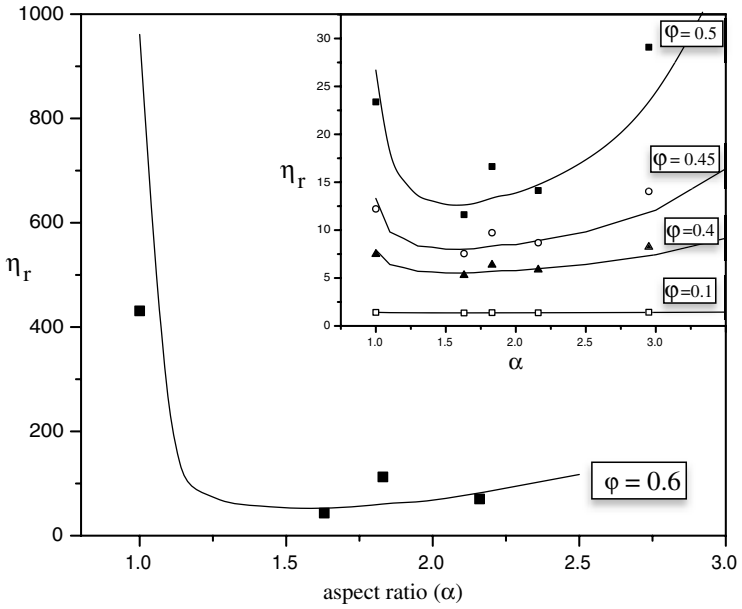

Figure 12. Conversion of maximum packing densities from figure 5 to relative viscosities as a function of aspect ratio using equation (8) for various particle volume fractions. The density maximum corresponds to a pronounced viscosity minimum. In the plot the symbols are obtained from experimental densities (figure 5) and the curves are derived, again using equation (8), from random packing densities from computer simulations.

hydrodynamic friction. For even higher aspect ratios A_g increases further, but now the packing density is dropping significantly such that the net effect for aspect ratio $\alpha = 4.4$ in figure 7 is a faster expansion than for spheres.

3.8. Effects on dynamics

The shape-dependent density maximum (figure 5) in the random packing of nearly spherical colloidal ellipsoids must also have a significant effect on the viscosity of such colloids. If colloids are arrested in a highly viscous, glassy phase because of geometrical constraints, it is very likely that a small change in colloid shape (at constant colloid concentration) will lower the viscosity substantially such that the glass 'melts' to a fluid in which the particles can escape from their arresting cages. This melting would be a consequence of the concentration dependence of the relative viscosity η_r which for high concentrations of randomly oriented particles follows the scaling [26]

$$\eta_r = \left(1 - \frac{\phi}{\phi_{max}}\right)^{-2}, \tag{8}$$

where ϕ_{max} is the colloid volume fraction at which the viscosity diverges. The precise form of the concentration dependence in equation (8) is not relevant; the argument here only requires a very steep viscosity increase on approach of ϕ_{max} which is approximately (presumably somewhat below) the random packing density. The prediction from equation (8) is that the viscosity of a sphere fluid will decrease when the spheres are deformed at constant colloid density until the aspect ratio is reached which has the maximum packing density (figure 12).

The viscosity will rise upon further elongating the colloids, and will continue to do so in the limit of thin rods where the random packing density follows the asymptotic result [7, 1]:

$$\phi_{\max}\alpha \sim \frac{c}{2}; \qquad \alpha \gg 1, \tag{9}$$

where $c \approx 10$ is the average contact number per rod [7, 8]. The viscosity change for aspect ratios near the packing density maximum will be modest for colloid volume fractions below about $\phi \approx 0.4$, but quite significant for dense fluids (figure 12). The effect of aspect ratio on viscosity has been verified experimentally for thin fibers (see the review in [7]). However, we have not been able to verify yet the viscosity change for dense fluids of our silica ellipsoids; it is difficult to measure high viscosities for such small samples (figure 1) and, moreover, it is not trivial to prepare samples with constant volume fraction.

4. Conclusions and outlook

In conclusion, we have quantitatively analyzed the random packing densities of ellipsoidal silica colloids as a function of their aspect ratio, and compared them with recent computer simulations. Our findings show that prolate colloids randomly pack more densely than spheres when their aspect ratio is lower than about 2.5. Confocal microscopy on a typical packing of (optically matched) ellipsoids, prepared by rapid sedimentation, shows that there is no long-range positional and orientational order: the silica ellipsoids very much randomly pack as in the computer simulations of the packing process. The colloidal stability of the ellipsoids is not only demonstrated by the reproducibility of the packing experiments but also by the slow expansion of the sediments against gravity. The trend in the expansion rate as a function of particle aspect ratio manifests the random packing density maximum and the density decrease at higher aspect ratios. The existence of the density maximum also suggests a drastic viscosity change (melting of glass) which can occur by slightly deforming the spherical shape in a sphere glass.

Acknowledgments

We thank Mark Klokkenburg for performing digital image analysis. This work is sponsored by NWO/Chemical Sciences and FOM.

References

[1] Williams S R and Philipse A P 2003 *Phys. Rev.* E **67** 051301
[2] Donev A, Cisse I, Sachs D, Variano E A, Stillinger F H, Connelly R, Torquato S and Chaikin P M 2004 *Science* **303** 990–3
[3] Bernal J and Mason J 1960 *Nature* **188** 910–1
[4] Frenkel D, Lekkerkerker H N W and Stroobants A 1988 *Nature* **332** 822–3
[5] van der Kooij F M, Kassapidou K and Lekkerkerker H N W 2000 *Nature* **406** 868–71
[6] van der Kooij F M and Lekkerkerker H N W 1998 *J. Phys. Chem.* B **102** 7829–32
[7] Philipse A P 1996 *Langmuir* **12** 1127–33 + corrigendum 1996
[8] Blouwolff J and Fraden S 2006 *Europhys. Lett.* **76** 1095–101
[9] Thies-Weesie D M E, Philipse A P and Kluijtmans S G J M 1995 *J. Colloid Interface Sci.* **174** 211–23
[10] Sacanna S, Rossi L, Kuipers B W M and Philipse A P 2006 *Langmuir* **22** 1822–7
[11] 2006 Soft Imaging System www.soft-imaging.net
[12] Henry D C 1931 *Proc. R. Soc.* A **133** 106
[13] Crocker J C and Grier D G 1996 *J. Colloid Interface Sci.* **179** 298–310
[14] Dullens R P A, Mourad M C D, Aarts D G A L, Hoogenboom J P and Kegel W K 2006 *Phys. Rev. Lett.* **96** 028304
[15] Wouterse A, Williams S R and Philipse A P 2007 submitted

[16] Perram J W and Wertheim M S 1985 *J. Comput. Phys.* **58** 409–16
[17] Ocaña M, Morales M P and Serna C J 1999 *J. Colloid Interface Sci.* **212** 317–23
[18] Beresford-Smith B, Chan D Y C and Mitchell D J 1985 *J. Colloid Interface Sci.* **105** 216–34
[19] Verwey E and Overbeek J 1948 *Theory of the Stability of Lyophobic Colloids* (New York: Elsevier)
[20] Koenderink G H, Sacanna S, Pathmamanoharan C, Rasa M and Philipse A P 2001 *Langmuir* **17** 6086–93
[21] Nowak E R, Knight J B, Ben-Naim E, Jaeger H M and Nagel S R 1998 *Phys. Rev.* E **57** 1971
[22] Knight J B, Fandrich C G, Lau C N, Jaeger H M and Nagel S R 1995 *Phys. Rev.* E **51** 3957
[23] Philipse A 2005 Particulate colloids: aspects of preparation and characterization *Fundamentals of Interface and Colloid Science* vol 4, ed J Lyklema (Amsterdam: Elsevier)
[24] Kozeny J 1927 *Sitz. ber. Akad. Wiss., (Wien)* IIa **136** 271–306
[25] Pathmamanoharan C and Philipse A P 1993 *J. Colloid Interface Sci.* **159** 96–107
[26] Kitano T, Kataoka T and Shirota T 1981 *Rheol. Acta* **20** 207